

Model-based Hydraulic Impedance Control for Dynamic Robots

Thiago Boaventura^{1,2}, Jonas Buchli¹, Claudio Semini², Darwin G. Caldwell²

Abstract—Ever more robots are designed to interact with the environment, including humans and tools. Legged robots, in particular, have to deal with environmental contacts every time they take a step. To handle these interactions properly, it is desirable to be able to set the robot's dynamic behaviour, i.e. its impedance. In this contribution, we investigate the most relevant theoretical and practical aspects in impedance control using hydraulic actuators, ranging from the force dynamics analysis and model-based controller design to the overall stability and performance assessment. We present results with one leg of the quadruped robot HyQ and also highlight the influence of hardware parameters, such as valve bandwidth and inertia, in the impedance and force tracking. In addition, we demonstrate the capabilities of HyQ's actively-compliant leg by experimentally comparing it with a passively-compliant version of the same leg. With such a broad spectrum of analyses and discussions, this paper aims to serve as a practical and comprehensive guide for implementing high-performance impedance control on highly-dynamic hydraulic robots.

I. INTRODUCTION

An increasing number of robots have to interact with the environment around them, with humans, tools or other objects. Physical contacts are inherent to many robotics applications such as assembly, service tasks, manipulation, and legged locomotion. To properly handle these physical contacts, especially in poorly structured environments, it is essential to be able to control the interaction forces, or more generally speaking, to control the robot's impedance, that is, the dynamic relation between the motion imposed by the contacts and forces the robot generates in response at the contact point.

To control of the robot's impedance means that a vast range of dynamic behaviors may be produced [1]. For instance, it is possible to emulate complex components such as nonlinear springs and dampers and to virtually place them anywhere within the robot's mechanical structure [2]. Also, we can change the component's characteristics (e.g. spring stiffness) on-the-fly while performing a certain task. Besides significantly increasing the robot's versatility, this ability to adjust the robot's impedance in real-time is also important for increased robustness of legged machines.

A proper choice of the structure of the impedance controller brings additional benefits to the robot's overall control. When a high-performance nested torque controller is present in the impedance control architecture (see Fig. 1), it is possible to straightforwardly exploit advanced high-level controllers that take care, for instance, of the robot's balance and vision. Model-based approaches such as operational space control [3]

¹ T. Boaventura and J. Buchli are with the Agile & Dexterous Robotics Lab, ETH Zürich. tboaventura@ethz.ch, buchlij@ethz.ch

² C. Semini and D. G. Caldwell are with the Department of Advanced Robotics, Istituto Italiano di Tecnologia (IIT). claudio.semini@iit.it, darwin.caldwell@iit.it

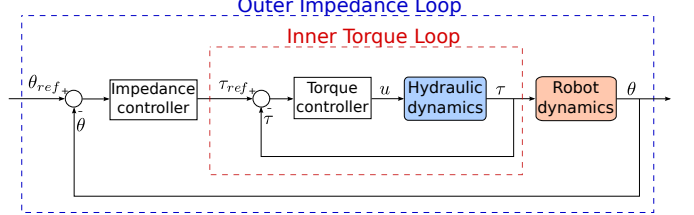


Fig. 1. Cascade impedance control architecture: an outer loop feeds back the position and creates the torque reference τ_{ref} for the inner torque loop, which calculates the input u to the valve. Both outer and inner controllers can use state feedback in case a model-based controller is employed.

and rigid body inverse dynamics feed forward control [4] can also be easily implemented. These controllers not only set the robot's desired dynamic behaviour, but are also crucial to enhance both its robustness in rough terrain locomotion [5] and its safety when interacting with the environment and people [6]. Such features are not only desirable but essential for legged robots that aim to walk over complex underground.

All the high-level controllers mentioned above produce torques as their command output. Thus, their performance depends directly on the torque tracking capabilities of the nested controller. To maximize the performance of the inner torque controller, it is essential to understand the basic principles behind force dynamics and to use this knowledge to design model-based controllers. Whereas some concepts, such as natural velocity feedback, are common and inherent to any actuation system that performs force control [7], there are other actuation dependent aspects, such as pressure nonlinearities in hydraulic actuators, that can also be taken into account to obtain better closed-loop performance.

In this contribution we will present the whole development of the impedance controller of the actively-compliant quadruped robot HyQ [8]. We emphasize that the controllers presented here may be beneficial not only to legged robots, but also to other dynamic systems. Both controllers and analyses are, in principle, valid for any kind of system that is able to feed back force/torque and position signals. This paper builds upon our previous work [9], [7], [10], [11], and its main focus is to provide a practical and comprehensive guide for designing and implementing high-performance impedance control on highly-dynamic hydraulically-actuated robots. In light of this focus, the main contributions are: (a) it summarizes and discusses all the most relevant theoretical and practical aspects of active impedance using hydraulic actuators, ranging from the force dynamics model analysis and inner loop design to the overall impedance controller stability and performance assessment; (b) it highlights the impact that the valve bandwidth can have on the closed-loop force bandwidth and stability margins, complementing the outcomes presented in [10]; and

(c) it experimentally shows the influence of the load inertia in the force tracking performance. In addition, we also experimentally demonstrate that a completely actively-compliant leg can emulate the compliant behaviour of a passive leg, as we initially showed in [10], extending the result analysis by showing in detail the stiffness tracking during high-frequency impacts; we critically list and discuss the advantages and disadvantages of active impedance; and finally, we extend the natural velocity feedback analysis and compensation design, initially investigated for the hydraulic force in [7], to the total load force, which includes the cylinder friction force.

The article is organized as follows. Section II presents a brief literature review, while Section III introduces the HyQ robot. In Section IV we introduce an important and intrinsic phenomenon in force dynamics: the natural velocity feedback. In the same section we present a new modelling framework for the force dynamics based on the transmission stiffness. In Section V we use modelling knowledge to present different approaches to the design of both inner and outer control loops in a cascaded impedance control architecture. Next, we investigate in Section VI the influence of the actuator bandwidth on the stability and performance of the closed-loop force controller, and in Section VII we present and discuss some experimental results and practical hardware issues. Finally, we summarize the main outcomes of this contribution in Section VIII together with a brief outline of future work.

II. RELATED WORK

Impedance at the end-effector (or contact point) can be achieved in two ways: *passively* or *actively* [12], [13]. *Passive impedance* is obtained through hardware and can be attributed to physical elements such as springs, dampers, the limited stiffness of the robot's links, or the compliance of the actuator transmission (e.g. gearboxes, harmonic drives, hydraulic oil, air, etc). On the other hand, *active impedance* is usually achieved via the control of the joint torques, regardless of additional passive elements.

A way to implement passive impedance on robotic devices has been found in reducing the transmission stiffness initially by using flexible sensors, and more recently by introducing springs in series with the actuator [14]. Besides reducing the transmission stiffness and making the force dynamics less reactive, the spring in series elastic actuators (SEAs) has also four other important functions: (a) to protect the actuator (or gearbox) from damage due to impact forces, (b) to store energy, (c) to be backdrivable and possibly safer during human-robot interaction, for instance, and (d) to measure the load force through the spring deflection. The design of SEAs requires a trade-off between robustness and task performance. To choose the most appropriate spring stiffness is not a trivial task and it can seriously limit the robot versatility. In order to avoid this trade-off, several variable stiffness actuators (VSAs) have been recently proposed [15]. Although VSA is a promising solution for compliant robots, aspects such as weight, volume, mechanical complexity, robustness, and velocity saturation still limit its use in highly-dynamic robots.

In contrast to passive-impedance-based systems, actively-compliant mechanisms rely on an analog or digital controller

to handle interactions. The work presented in [1] describes the physical foundation of *impedance control* for articulated manipulators. It emphasizes that two physical systems *must* physically complement each other during dynamic interactions. That is, along any degree of freedom, if one system is an impedance, the other must be an admittance and vice versa. However, there are several other techniques for controlling manipulator impedance. For instance, in [3] the concept of *operational space control* is presented. In this framework, the focus of control is shifted from the single joints of the robot to the actual task, typically at the end-effectors. More recently, the very intuitive *virtual model control* [2] was presented for legged locomotion. In this framework, virtual components that have physical counterparts, such as mechanical springs and dampers, are placed at convenient locations within the robot or between the robot and the environment.

A common control architecture used to implement an impedance controller is depicted in Fig. 1 [16], [17]. However, there are also other control schemes, such as position-based impedance control (i.e. admittance control) [18], [19], that can be employed. Despite the control scheme, when implementing an impedance controller on a robotic system, force feedback and force control are critical to achieve a robust and versatile behaviour in poorly structured environments, as well as safe and reliable operation in the presence of humans [20].

There are several reasons for stability problems in force control, such as structural modes, transmission stiffness, actuator bandwidth, load dynamics, and actuator backdrivability [21]. While a softer transmission stiffness (e.g. in SEAs) is able to avoid some of the stability challenges, it also reduces the overall system bandwidth. Thus, to boost the force tracking capabilities of the system, the transmission stiffness should not be intentionally reduced and high-bandwidth actuators should be used. We will more deeply discuss these points in Section VI. Good actuator backdrivability is always desirable since it permits to improve the closed-loop force control accuracy [22]. In addition, advanced model-based controllers can be employed to compensate for the structural flexibility and load dynamics. The load dynamics compensation was initially discussed for hydraulic actuators in [23], followed by several other works which demonstrated that closed-loop force control is ineffective without a velocity feed forward command that compensates for a *natural velocity feedback* [24], [25]. In [7] we have shown that this natural velocity feedback is intrinsic to the force control problem no matter the actuation system that is used.

Besides the performance, the stability and robustness of the active impedance controller is also a fundamental issue that must be analysed. To ensure a stable contact between the environment and an actively-compliant leg, the leg's impedance controller has to be passive at the interaction point. The range of achievable impedance parameters that keep the system passive is often called the *Z-width* (where *Z* stands for impedance) [26], [27]. Although the Z-width for virtual environments has been intensively investigated for haptics devices, to the best of our knowledge, [10] is the only study on the achievable range of impedances for virtual components in legged robots, and that considers the torque closed-loop

bandwidth impact in such a range. In this paper we will extend this previous study by showing the impact of the valve dynamics on the closed-loop torque bandwidth.

Before going into the design of the controllers, we will present in the next section the hydraulically-actuated robot, HyQ, and quickly explain its mechanical design and the reasons for having chosen hydraulics as the actuation system.

III. HYQ HARDWARE OVERVIEW

HyQ, Fig. 2(a), is a versatile quadruped robotic platform built at the Istituto Italiano di Tecnologia to perform actions that range from slow, precise and deliberate to highly-dynamic [8]. To obtain the flexibility needed to accomplish such different tasks, HyQ was designed to have robust mechanical performance and advanced control capabilities.

HyQ has 12 hydraulically actuated joints, weighs 75kg, and has the following dimensions: $1\text{ m} \times 0.5\text{ m} \times 1\text{ m}$ ($L \times W \times H$). All these joints have magnetic absolute and optical relative encoders (80000 counts per revolution), as well as strain gauge based force/torque sensors. In addition, there are pressure sensors that measure the supply and return pressures and an Inertial Measurement Unit (IMU) on the torso. HyQ's feet are formed from a highly compressed rubber (resembling tyre rubber) which gives the robot good ground traction. In addition, this material provides slight filtering of high-frequency impact forces during dynamic tasks (e.g. trotting).

Each of HyQ's legs has three active rotational degrees of freedom (DOF): the hip abduction/adduction (HAA) joint, the hip flexion/extension (HFE) joint, and the knee flexion/extension joint (KFE), as depicted in Fig. 2(b). More details on the robot design, kinematics and dimensions can be found in [8]. All the joints are actuated by high-speed servovalves connected to hydraulic asymmetric cylinders (HFE and KFE) and semi-rotary vane actuators (HAA). These joints provide high speed and torque for motions in both the sagittal and frontal plane of the robot. The hydraulic supply pressure p_s is set to $p_s = 180$ bar, and the maximum flow of the off-board pump is about 30 L/min.

Hydraulic actuation has many properties that make it an ideal choice for highly dynamic articulated robot applications. Firstly, hydraulic actuators are strong and fast. Also, they are mechanically simple and robust. No gearboxes are necessary for increasing the torque capabilities, and hydraulic

actuators can handle high impact forces more robustly than geared electric motors. In addition, they have a substantially higher power-to-weight ratio than electric drives [28]. Also, in contrast to the widespread idea that hydraulics is difficult to control, we will show that hydraulic actuators have sufficiently high bandwidth such that, combined with rather simple model-based controllers, they guarantee high-performance torque control and accurate regulation of the robot impedance in a wide range.

The main drawback of today's hydraulic actuation is the low energy efficiency. However, due to the significant advantages of this actuation, the low energy efficiency is tolerable for HyQ. Improving the energy efficiency is part of the on-going work with the robot [29].

IV. TRANSMISSION COMPLIANCE EFFECT

Before designing any controller, it is fundamental to understand the dynamics of the control objective, i.e. the quantity to be controlled. Thus, in this section we will introduce some basic principles behind the force dynamics.

First of all, due to causality reasons, it is important to highlight that force is always controlled over a transmission element that is deformable or compressible. The force is transmitted from the actuator to the load through this compliant transmission element, which can be modelled as an impedance and, due to causality reasons, it must have velocities as input and force as output [1]. Therefore, it is possible and convenient to represent the force dynamics through the following 3 generic elements: a velocity source (i.e. the actuator), a transmission (compliant element between actuator and load), and a load [7].

Using these 3 elements, we can model the force f_{a2l} transmitted from the actuator to the load as $\dot{f}_{a2l} = K_t(\dot{x}_a - \dot{x}_l)$, being \dot{x}_a and \dot{x}_l the actuator and load velocities respectively and K_t the transmission stiffness. This way of modelling the force has the strong advantage of explicitly exposing an important physical phenomenon in force control that is intrinsic to any actuator type: a natural feedback of the load velocity \dot{x}_l into the force dynamics. Since the \dot{x}_l dynamics clearly depends on the characteristics of the load itself (e.g. inertia, friction, etc), it means that also the dynamics of \dot{f}_{a2l} and consequently the force control tuning and performance depends on how the load looks like. In hydraulics, the actuation system supplies velocity to the load through fluid flow. Thus, the velocity source can be considered the pump and valve together. To define a hydraulic transmission stiffness, we will first derive the traditional hydraulic force model.

The hydraulic force f_h consists of a balance between the forces created in the actuator chambers a and b . Neglecting external and internal leakages, the mass conservation principle can be applied to each of the chambers by using the continuity equation, and the following well-known expression for the hydraulic force dynamics can be written [30]:

$$\dot{f}_h = \frac{A_p \beta_e}{v_a} (q_a - A_p \dot{x}_p) - \frac{\alpha A_p \beta_e}{v_b} (-q_b + \alpha A_p \dot{x}_p) \quad (1)$$

where A_p is the piston area and α the cylinder chambers area ratio (i.e. $A_a = A_p$ and $A_b = \alpha A_p$), β_e is the bulk modulus

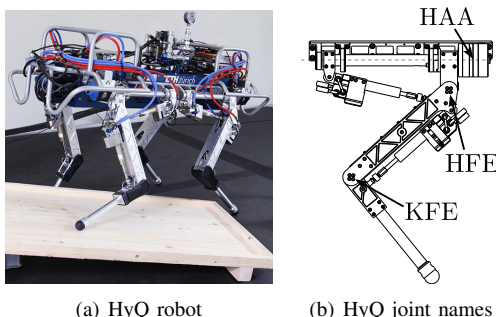


Fig. 2. (a) The HyQ robot. The HyQ leg drawing in (b) defines the joint names: the hip abduction/adduction (HAA), the hip flexion/extension (HFE), and the knee flexion/extension (KFE).

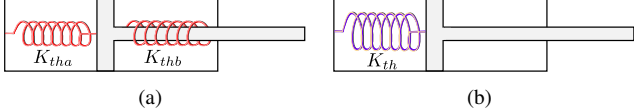


Fig. 3. Hydraulic stiffness represented by springs. (a): Hydraulic transmission springs for each chamber. (b): Equivalent hydraulic stiffness for the whole system, with stiffness K_{th} .

of the fluid, v_a and v_b the actuator chamber volumes, x_p the piston position, and q_a the fluid flow going into chamber a and q_b the flow going out of chamber b . In this modelling analysis the pipe line volume V_{pl} is already accounted into the respective chamber volume (e.g. $v_a = A_p x_p + V_{pl}$ and $v_b = \alpha A_p (L_c - x_p) + V_{pl}$, being L_c the cylinder length). Eq. 1 can be easily re-written to better match the modelling framework we described above. This way each actuator chamber would define a transmission stiffness ($K_{tha} = A_p \beta_e / v_a$ and $K_{thb} = \alpha A_p \beta_e / v_b$, Fig. 3(a)), which can then be modelled as parallel springs to obtain a resultant hydraulic stiffness (Fig. 3(b), $K_{th} = K_{tha} + K_{thb} = A_p \beta_e (1/v_a + \alpha/v_b)$). That is:

$$\dot{f}_h = K_{tha}(q_a - A_p \dot{x}_p) - K_{thb}(-q_b + \alpha A_p \dot{x}_p) = K_{th}(q_e - A_e \dot{x}_p) \quad (2)$$

where $q_e = \frac{v_b q_a + \alpha v_a q_b}{v_b + \alpha v_a}$ is the equivalent flow rate, and $A_e = A_p \left(\frac{v_b + \alpha^2 v_a}{v_b + \alpha v_a} \right)$ the equivalent area. It is important to underline that by writing Eq. 2 in this form an important physical characteristic of the system is made explicit: the hydraulic transmission stiffness K_{th} , which is an essential physical quantity in the force dynamics. The stiffer the transmission, the faster the force dynamics. *A priori* knowledge of the transmission stiffness can give important insights into the robot's control and mechanical design [11].

By linearising Eq. 2 around an equilibrium point $P_\circ = (p_{a\circ}, p_{b\circ}, u_{v\circ}, x_{p\circ}, \dot{x}_{p\circ})$, we can obtain the block diagram shown in Fig. 4. The operator Δ represents the variation of a given quantity around the equilibrium value. In this diagram we can clearly see that the linearised piston velocity $\Delta \dot{x}_p$ is fed back as a flow into the open-loop force dynamics. Again, this natural feedback of the load velocity is intrinsic to the force dynamics no matter the actuation system used and it appears because the transmission that connects the actuator to the load will never be infinitely stiff. By neglecting the valve spool dynamics, the hydraulic force transfer function can be written based on the block diagram of Fig. 4 as:

$$\frac{\Delta f_h(s)}{\Delta u_v(s)} = \frac{K_{th\circ} K_{qe} (M_l s + B_l + B)}{(M_l s + B_l + B) \left(s - \frac{K_{th\circ} K_{ce}}{A_p} \right) + K_{th\circ} A_{e\circ}} \quad (3)$$

where M_l and B_l are respectively the inertia and viscous friction coefficient of the load, B the viscous friction coefficient of the cylinder, u_v the valve input, $K_{qe} = \frac{v_{b\circ} K_{qa} + \alpha v_{a\circ} K_{qb}}{v_{b\circ} + \alpha v_{a\circ}}$ the equivalent flow gain and $K_{ce} = \frac{1}{1+\alpha^2} \left(\frac{v_{b\circ} K_{ca} - \alpha^3 v_{a\circ} K_{cb}}{v_{b\circ} + \alpha v_{a\circ}} \right)$ the equivalent flow-pressure coefficient, being K_q and K_c the well-known valve's flow gain and flow-pressure coefficient for the chambers a and b [30]. Nonlinear friction terms such

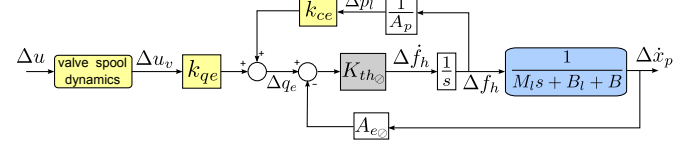


Fig. 4. Block diagram for the open-loop *linearised hydraulic force*. The blocks related to the valve are depicted in yellow, the load in blue, and the transmission stiffness in gray. Also, $p_l = p_a - \alpha p_b$ represents the load pressure, and u the valve command. The piston velocity $\Delta \dot{x}_p$ is multiplied by the equivalent area $A_{e\circ}$ and is transformed into a flow. This flow is then fed back into the force dynamics, representing an intrinsic velocity feedback.

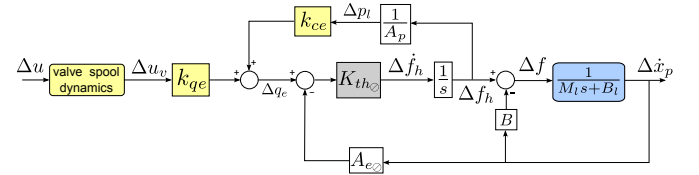


Fig. 5. Block diagram for the open-loop *load force dynamics*. Differently from the hydraulic force shown in Fig. 4, for the load force there are two paths where the velocity influences the load force dynamics: one through $A_{e\circ}$ and another through the viscous friction B in the hydraulic cylinder.

as Coulomb and static friction were neglected in this linear analysis for sake of simplicity and because on HyQ their effects are not significant during dynamic motions [11].

The *hydraulic force* f_h , however, is not the force that is directly acting on the load. The effects of viscous friction, which are very significant in hydraulic actuators due to their tight sealing to avoid internal leakage, cannot be neglected and a *load force* f can be defined ($f = f_h - B \dot{x}_p$). The actuator friction terms can be experimentally defined by measuring the pressures p_a and p_b , the load force f and velocity \dot{x}_p . The velocity framework can also be applied to the load force, which is in practice the physical quantity that is being measured and controlled in the HyQ leg to achieve active impedance. The linearised load force dynamics can be written, based on Fig. 5, as follows:

$$\frac{\Delta f(s)}{\Delta u_v(s)} = \frac{K_{th\circ} K_{qe} (M_l s + B_l)}{(M_l s + B_l + B) \left(s - \frac{K_{th\circ} K_{ce}}{A_p} \right) + K_{th\circ} A_{e\circ}} \quad (4)$$

As we can see in Eq. 3 and Eq. 4, there is a zero in the transfer function, usually located at low frequencies, which would limit the performance of a simple error feedback controller, such as a PD-controller. Thus, we will use the models presented in this section to derive, in the next section, model-based force controllers which are able to eliminate the influence of this zero and achieve better tracking performances.

V. COMPLIANT CONTROLLER DESIGN

The main goal of the impedance control for the HyQ robot is to actively generate a compliant behaviour through a rigid structure. It uses a cascade control architecture, as shown in Fig. 1, which consists of an outer position control loop that manipulates the reference input of an inner joint torque control loop.

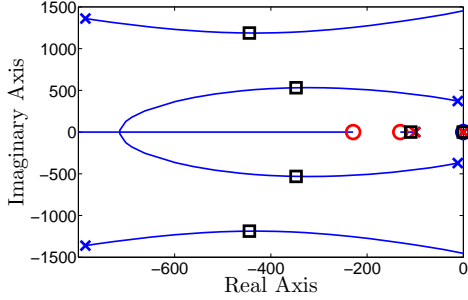


Fig. 6. Root locus for the closed-loop load force using a PID controller. The closed-loop poles are marked with black squares, the open-loop poles and zero in blue, and the controller poles and zeros in red. As seen, the open-loop system's zero, which is very close to the origin, creates a dominant closed-loop pole at very low frequencies which slows down the system response.

In this section we will investigate some possible control approaches for both inner and outer loops. In Section V-A we show why the force tracking performance is limited when using a PID controller and also how to improve the closed-loop force controller bandwidth by compensating for the natural velocity feedback. Note that throughout this article the terms *force control* and *torque control* are used interchangeably.

A. Force Controller Design

The first step to control HyQ's impedance is the development of a high-performance force controller at the robot joints. This controller permits to adjust both the interaction forces at the robot's end-effector and the joint torques. Furthermore, the implementation of a precise force controller gives HyQ the attractive possibility to consider its joints as high-fidelity torque sources. This capacity is very convenient when implementing many other high-level controllers. Also, since many robots can well be modelled as multi-rigid-body-systems, their dynamics naturally have torques as their inputs. Therefore, the implementation of tasks such as trotting [31], jumping [9], balancing and orientation [32] become much more intuitive and easy with a low-level torque controller.

To obtain a good closed-loop force performance can be challenging with hydraulics due to the very small compressibility of mineral oil. This causes the pressure and consequently force dynamics to have a high stiffness and thus a high gain, requiring a very fast flow controller. The key features for achieving high-performance torque control with a hydraulic system are: *a)* to use servovalves with a high flow control bandwidth¹ to exploit the naturally high hydraulic stiffness and *b)* to improve the torque controller performance using model-based control. Next, we will present 3 different control approaches for the inner force loop.

1) PID Controller: It is well known that a PID controller alone does not provide good performance when controlling forces [25] due to the zero in the open-loop force transfer function (Eq. 3 and Eq. 4).

Considering that the variable to be controlled is the linear load force Δf (Eq. 4), we can close the force loop using a

¹HyQ uses fast valves with bandwidth of about 250 Hz for displacements in the range of $\pm 25\%$ of the total spool range of motion [33].

PID controller and obtain the root locus shown in Fig. 6. The poles and gains from the open-loop force transfer function are displayed in blue, and those from the controller in red. The closed-loop poles are marked with black squares. As we see in Fig. 6, there is a dominant closed-loop pole at very low frequency, close to the origin. This pole slows down significantly the system response and the settling time can drastically increase. Practically, it means that the open-loop zero cancels out the effect of the controller integrator and a PID controller behaves as a PD controller and the system will always present an error in steady-state that is inversely proportional to the load inertia and friction [11].

2) Velocity compensation + PID controller: As we have seen, the dynamics of the force that is transmitted from the actuator to the load depends not only on the actuator but also on the load dynamics itself (e.g. mass and friction). The load dynamics introduces a zero into the force transfer function (see Eq. 4), which limits the achievable force bandwidth when using a PID controller. In this section, we present a feed forward controller which aims to cancel out the load dynamics influence and to increase the force tracking performance. This feed forward controller is targeted at dynamic applications where fast reactions and high speeds are required, and it is used together with a force feedback PID controller.

The goal of the velocity compensation feed forward controller is to provide a valve command that virtually cancels the natural loops created by the load velocity feedback, which can be clearly seen in Fig. 4 and Fig. 5. By providing this feed forward command, the effect of the velocity loop on the system can be compensated for (i.e. the velocity feedback loop can be virtually opened). In terms of system modelling, this compensation results in a perfect zero/pole cancellation [7]. *To cancel out the influence of the load zero in the force dynamics is the main goal of the load velocity compensation.* With this zero/pole cancellation, it is theoretically possible to increase the gains without making the system unstable, taking the dominant closed-loop pole to higher frequencies.

Unlike the hydraulic force f_h , the load force f has not only one but two feedback points in the system (compare Fig. 5 and Fig. 4). The compensation of the path where the velocity is fed back through the gain $A_{e\otimes}$ can be done similarly to the compensation performed in [7] for the hydraulic force. The final control effort u_{vc} that fully compensates for the load velocity can be written as:

$$u_{vc} = \frac{(A_{e\otimes} - BK_{ce})\Delta\dot{x}_p}{K_{qe}} + \frac{B\Delta\ddot{x}_p}{K_{qe}K_{th\otimes}} \quad (5)$$

As noticed, to eliminate the load motion from the load force dynamics requires also the piston acceleration $\Delta\ddot{x}_p$. Since the acquisition of this quantity in practice is generally through double numerical differentiation, it might be too noisy to be used. Thus, an approximation of u_{vc} shown in Eq. 5 could neglect the acceleration-dependent term. The effect of neglecting this term is presented in Fig. 7. As we can see, to neglect this term does not significantly influence the velocity-compensated system response. In Fig. 7 we also show the slow response which is characteristic of a simple

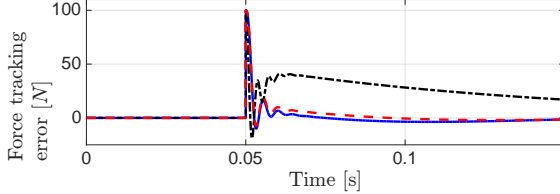


Fig. 7. Simulation of a 100 N step response of the load force f with a cylinder (viscous friction $B = 1000 \text{ Ns/m}$) moving a load of $M_l = 20 \text{ kg}$ and $B_{l\theta} = 10 \text{ Ns/m}$, cylinder. The solid blue line shows the force tracking error with the full velocity compensation ($\text{RMSE} = 8.28 \text{ N}$), the red dashed line neglects the acceleration term in the velocity compensation ($\text{RMSE} = 8.38 \text{ N}$), and the black dot-dashed line shows the error with a simple PID and no velocity compensation ($\text{RMSE} = 20.01 \text{ N}$).

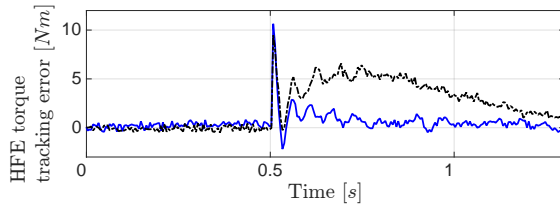


Fig. 8. Experimental result for a 10 Nm torque step in the HFE joint: in dashed black the non-compensated torque tracking error ($\text{RMSE} = 2.34 \text{ Nm}$), which uses only a PID controller, and in solid blue the compensated one ($\text{RMSE} = 1.13 \text{ Nm}$), which uses the feed forward command u_{vc} to enhance the PID control response. The velocity compensation made the system about 3 times faster and reduced the RMSE by about 50%.

PID force feedback controller with no feed forward velocity compensation (black dot-dashed line).

In terms of transfer function, the simplified load velocity compensation (i.e., when neglecting the acceleration term) does not cancel the zero with a pole, but the two complex conjugated poles from the hydraulic dynamics become real. This allows to further increase the closed-loop gain and consequently the system performance.

To demonstrate the effectiveness of the velocity compensation approach in practical force control applications, we performed an experiment with the HFE joint of the HyQ leg. A 10 kg weight was fixed to the end-effector to permit a torque step magnitude of 10 Nm. As we can see in Fig. 8, both *compensated* and *non-compensated* error responses resemble the simulation results shown in Fig. 7, that is, the PID response (non-compensated, black line) notably converges more slowly than when velocity compensation is applied.

3) *Feedback linearization controller:* Hydraulic flow dynamics is highly nonlinear [30], and so is the hydraulic force dynamics. Therefore, traditional linear controllers behave accordingly to the design specifications only when close to the equilibrium point. However, it is desirable that the controller performance indexes, such as rise time and overshoot, are satisfied for the whole range of operation of the nonlinear system and not only around the equilibrium point. To overcome this issue, an *input-output feedback linearization* controller can be used. In this approach, state feedback is used to linearize the relation between the control input and the controlled variable within the whole range of operation of the system.

Based on Eq. 2 and on the definition of the load force ($f = f_h - B\dot{x}_p$), and by modelling the chamber flows as $q_a =$

$K_v u_v \Delta P_a$ and $q_b = K_v u_v \Delta P_b$, where K_v is the valve gain and ΔP represents the pressure difference in the chamber (e.g. for $u_v > 0$ we have $\Delta P_a = p_s - p_a$ and $\Delta P_b = p_b - p_t$) [30], the load force dynamics can be written as:

$$\dot{f} = \mathbf{f}(x_p, \dot{x}_p, \ddot{x}_p) + \mathbf{g}(P, x_p) u_v \quad (6)$$

where $\mathbf{f}(x_p, \dot{x}_p, \ddot{x}_p) = -K_{tha}\dot{A}_e \dot{x}_p - B \ddot{x}_p$ and $\mathbf{g}(P, x_p) = K_v (K_{tha}\sqrt{\Delta P_a} + K_{thb}\sqrt{\Delta P_b})$.

With the load force dynamics represented in the form shown in Eq. 6, it is straightforward to calculate a valve command u_{FL} which compensates for the natural load velocity feedback in the entire operating range (and not only around the operating point) and for the pressure-flow nonlinearities as following:

$$u_v = u_{FL} = \frac{1}{\mathbf{g}(P, x_p)} (v - \mathbf{f}(x_p, \dot{x}_p, \ddot{x}_p)) \quad (7)$$

where v is a function that will determine the load force tracking error dynamics. By applying the control input u_{FL} described in Eq. 7 to the system in Eq. 6, the load force dynamics becomes $\dot{f} = v$. Choosing v as a PI controller with an additional feed forward term corresponding to the time derivative of the force reference (i.e. $v = \dot{f}_{ref} - K_p(f_{ref} - f) - K_i \int (f_{ref} - f) dt$), we obtain an ordinary differential equation for the force error dynamics (i.e. $\dot{e}_f - K_p e_f - K_i \int e_f dt = 0$, where $e_f = f_{ref} - f$) and then the gains K_p and K_i can be easily designed to satisfy the system requirements such as rise time and overshoot.

B. Impedance Control Design

The presence of an inner torque control loop, which can be designed using one of the 3 methods presented before, makes the implementation of an impedance controller easier. This impedance controller then calculates the torques needed to make the robot react according to a desired dynamic behaviour. In this section we will present two control approaches to set a desired robot impedance². The first one is designed in joint-space and the second one in task-space.

1) *PD joint-space position control + inverse dynamics controller:* The easiest way to implement an impedance controller is probably by closing a *PD joint-space position loop*. An integral term is usually not necessary because zero steady-state position error, in general, is not necessarily a design goal in a compliant system. Also, since most existing manipulators and robots are designed with rigid links [34], they can usually be well modelled as rigid body systems. Rigid body dynamics defines a relationship between the torques (or generalized forces) acting on the robot joints and the accelerations they produce. It accounts for the links inertia, gravity, and also Coriolis and centripetal forces [35].

Partial feedback linearization using inverse rigid body dynamics, or simply *inverse dynamics*, is a very powerful model-based control technique. The inverse dynamics controller calculates feed-forward torques τ_{ff} that are added to the feedback PD controller torques τ_{fb} and sent to the closed-loop torque control, as shown in Fig. 9. An immediate advantage of inverse dynamics control is that it allows for compliant and usually

²Dynamic relation between force and velocity.

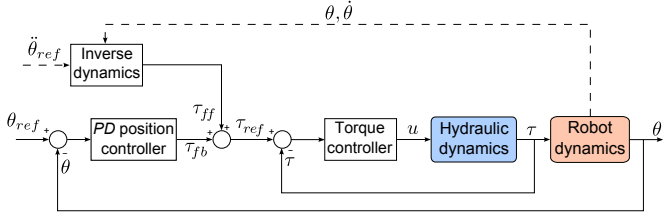


Fig. 9. Block diagram for the HyQ cascade control with an outer feedback joint-space position loop. It creates, together with a feed forward term from the inverse dynamics, the torque reference τ_{ref} for the inner torque loop. The model-based inverse dynamics controller needs the feedback of the joint position θ and velocity $\dot{\theta}$, and also the reference acceleration $\ddot{\theta}_{ref}$ to calculate the feed forward command τ_{ff} .

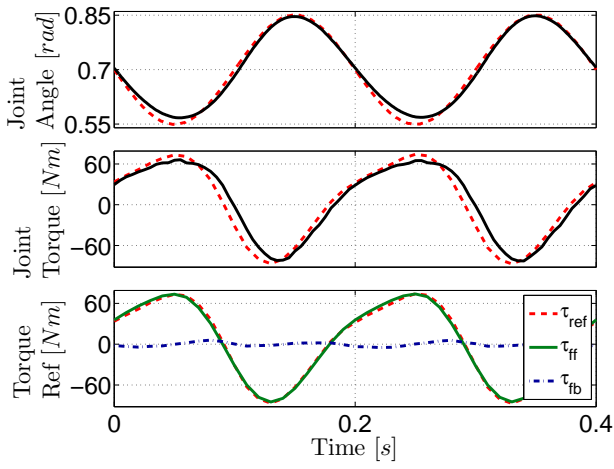


Fig. 10. Experimental results showing a precise position and force tracking for a 5 Hz sine position reference for the HFE joint. In the first two plots, the red dashed lines indicate the reference command and the black solid ones the actual value. The last plot shows that the reference torque τ_{ref} ($\tau_{ref} = \tau_{ff} + \tau_{fb}$) consists essentially of the feed-forward term τ_{ff} .

more robust legged locomotion since it permits to reduce the robot stiffness (i.e. PD joint position gains) without sacrificing position tracking performance. Having these capabilities is not only desirable but essential for locomotion in unstructured and partially unknown environments [5].

In Fig. 10 we demonstrate the inverse dynamics controller experimentally. It shows position and force tracking for the HFE joint for a 5 Hz sine motion performed with the leg fixed to a vertical slider. This experiment was performed with the feedback linearization force control approach (Section V-A3). The third plot shows the two components τ_{fb} and τ_{ff} of the torque reference. As we can see, τ_{fb} is very small. This highlights the accuracy of both the HyQ leg rigid body model and the torque controller for high joint velocities.

2) *Virtual Model Control:* The most intuitive way of setting a desired impedance profile for a robot is probably through virtual model control [2]. In this framework, virtual elements that have physical counterparts, for example mechanical springs, dampers, etc., are placed at points of interest within the reference frames of the robot. Once the placement is done, it is possible to define a Jacobian matrix, and map the interaction forces between these virtual components and the robot as desired joint torques τ_{ref} .

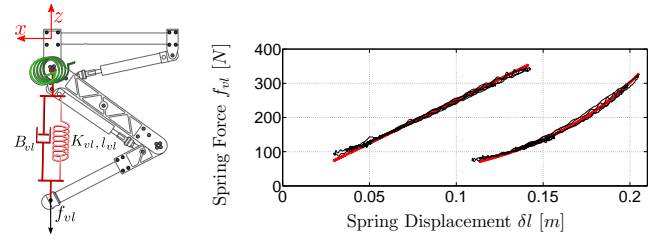


Fig. 11. (a) Virtual components implemented on the HyQ leg: a rotational spring-damper at HFE, and a linear spring-damper between the hip and the foot. The virtual leg damping is B_{vl} , the stiffness K_{vl} , and the virtual spring length l_{vl} . The force f_{vl} is created by these virtual components. The red arrows represent the coordinate frame axes x and z . (b) Two different virtual springs implemented on the real hardware: a linear one ($f_{vl} = 2500\delta l_{vl}$, being $\delta l_{vl} = l_{vl_0} - l_{vl}$, where l_{vl_0} is the free length of the virtual spring) and an exponential one ($f_{vl} = 16e^{15}\delta l_{vl}$). The red line represents the desired stiffness profile, and the black line the one produced by the HyQ leg.

In this approach, to make HyQ actively compliant we used a virtual spring-damper between the HFE and the foot, as depicted in Fig. 11(a). The spring stiffness can easily assume any programmable characteristic, such as linear ($f_{vl} = K_{vl}\delta l_{vl} + B_{vl}l_{vl}$) or exponential ($f_{vl} = f_{vl_0}e^{K_{vle}\delta l_{vl}}$, where K_{vle} is the exponential stiffness gain [$1/m$]). Fig. 11(b) shows experimental results that demonstrate HyQ's impedance tracking capabilities.

For all the impedance control approaches presented in Section V-B, it is still not clear how to choose the most suitable virtual leg stiffness and damping. It might depend on the terrain characteristics as well as on the task (e.g. walking, running, trotting). Learning and optimization can also be applied to find the most suitable leg impedance [36]. However, this topic must be further investigated to improve the performance of legged robots in general.

Although it is not clear how to choose the most suitable robot impedance, we can at least set limits for both stiffness and damping to ensure that the robot will stably interact with the environment, which is in general passive (i.e. it does not transfer extra energy to the robot) [10].

VI. RELATION BETWEEN FORCE CONTROLLER STABILITY AND PERFORMANCE & ACTUATOR BANDWIDTH

In the previous sections we presented some control approaches that can be used to implement high-fidelity impedance controllers through the cascade scheme shown in Fig. 1. With such scheme, the outer impedance loop performance depends directly on the inner loop tracking capabilities. Therefore, the first step towards the implementation of a high-fidelity impedance control is to enhance the inner force loop performance. In light of these considerations, we will discuss in this section how the valve bandwidth can be used to improve the inner loop performance and stability, and consequently the overall compliant behaviour on hydraulic systems.

To assess the impact of the valve bandwidth on the force closed-loop controller, we will consider the velocity compensation approach described in Section V-A2 since it is simple and effective. For sake of simplicity, the feedback controller will be reduced to a simple proportional (P) controller. This

leads to the control law $u = k_p e_f + u_{vc}$, where k_p is the proportional force gain, $e_f = f_{ref} - f$ is the force tracking error, and u_{vc} the feed forward velocity compensation command shown in Eq. 5.

Based on Eq. 4, and taking into account a second order valve dynamics, the open-loop transfer function between the valve command u and the actuator force f can be defined as:

$$G(s) = \frac{\Delta f(s)}{\Delta u(s)} = \left(\frac{1}{\frac{1}{\omega_v^2} s^2 + \frac{2D_v}{\omega_v} s + 1} \right) \frac{\Delta f(s)}{\Delta u_v(s)} \quad (8)$$

where $\omega_v = 2\pi f_v$ is the valve spool natural frequency, and D_v the valve spool damping.

$K(s)$ being the controller transfer function, the open-loop transfer function from f_{ref} to f can be defined as $H_{OL}(s) = K(s)G(s)$ and the closed-loop one as $H_{CL}(s) = H_{OL}(s)/(1 + H_{OL}(s))$. Considering a perfect velocity compensation, both H_{OL} and H_{CL} result in 3rd order systems.

To investigate the stability and performance of the closed-loop system, we will use the concepts of *bandwidth* and *phase margin*. Bandwidth is a natural specification for system performance, and is defined as the frequency $\omega_{BW} = 2\pi f_{BW}$ where the magnitude of the transfer function is -3 db. Phase margin is used to indicate the stability margins of the system, and it is defined as the amount by which $G(j\omega)$ exceeds -180 deg when $|H_{OL}(j\omega)| = 1$, being $s = j\omega$. For tuning k_p we used as design criteria a phase margin of $PM = 60$ deg, which produces a fast non-oscillatory response.

While for a third order system an analytical solution of the bandwidth and phase margin would not be very illustrative, numerical analyses can be used to obtain the relation among the closed-loop torque bandwidth, the bandwidth of the actuator (in this case the valve), and the phase margin. Nevertheless, to enhance our understanding about this relation, we also investigated several analytical approximations for the bandwidth, which are based on reduced-order models [37], [38]. The analytical bandwidth that gave the best approximation of ω_{BW} for the given PM constraint ($PM = 60$ deg) was the following ω_{BW_2} , which is based on a second order approximation of H_{CL} [37]:

$$\omega_{BW_2} = \frac{\omega_v(2D_vK_{ce}K_{th} - A_p\omega_v)}{K_{ce}K_{th} - 2A_pD_v\omega_v} \quad (9)$$

The numerical bandwidth f_{BW} of $H_{CL}(jw)$ and its second order approximation f_{BW_2} , both in Hz, are shown in Fig. 12 for two different situations. Their magnitudes can be seen in the left y-axis, while on the right y-axis we show the phase margin PM of the open-loop system $H_{OL}(jw)$. In Fig. 12(a) we tuned the gain k_p with a valve of bandwidth $f_v = 150$ Hz (note that for $f_v = 150$ Hz we have $PM = 60$ deg), while in Fig. 12(b) we tuned it with a valve of $f_v = 250$ Hz.

The most interesting outcome of these plots is that, for a given controller gain k_p , f_{BW} has a very non-linear profile, and higher valve bandwidths f_v per se are not able to increase the closed-loop bandwidth much and can actually considerably decrease it. On the other hand, a higher valve bandwidth f_v always yields more phase margin, as we can notice in both plots. For instance, Fig. 12(a) shows that for $f_v = 250$ Hz

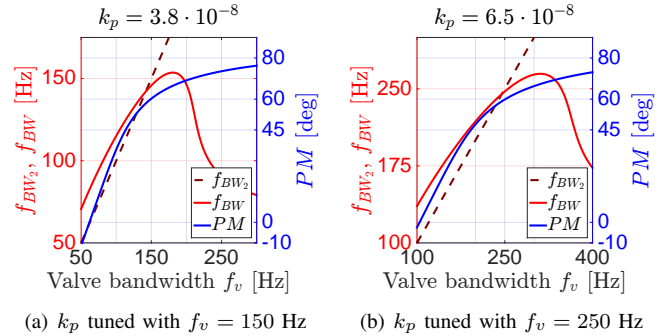


Fig. 12. Both plots show: on the left y-axis the numerical evaluation of the closed-loop force control (H_{CL}) bandwidth f_{BW} (solid red line) and its second order approximation f_{BW_2} (dashed brown line, calculated using Eq. 9), both in Hz; and on the right y-axis the phase margin (solid blue line) of the open-loop system (H_{OL}). In (a) the gain k_p (shown at the top of each plot) was tuned with a valve of $f_v = 150$ Hz, while in (b) a faster valve of $f_v = 250$ Hz was used to tune it. In both cases k_p was tuned using the criteria of $PM = 60$ deg (note that for $f_v = 150$ Hz in (a) and $f_v = 250$ Hz in (b) we have $PM = 60$ deg). The estimation f_{BW_2} is more accurate around the value of f_v used to tune k_p . The key fact to notice is that, for a given force control gain k_p , a higher valve bandwidth f_v enlarges the phase margin PM . This permits to set a higher k_p value thus increasing the closed-loop bandwidth ω_{BW} .

we would have $PM = 75$ deg if we would keep $k_p = 3.8 \cdot 10^{-8}$. This higher phase margin allows us then to increase the feedback controller gain k_p so that we keep having the same response characteristics (i.e. $PM = 60$ deg). Finally, it is this higher k_p that will be able to more significantly increase the closed-loop bandwidth, as we can see in Fig. 12(b).

As a conclusion, we can say that *higher valve bandwidths are able to increase the force controller stability margins and/or the closed-loop force controller bandwidth*. This outcome matches and complements the results we have already obtained in [10] for the closed-loop impedance controller of the Multiple-Input-Multiple-Output (MIMO) HyQ hydraulic leg, that is:

- for a given cascade impedance control, the higher the inner torque loop gains (e.g. k_p), the smaller the stable range of impedances (Z-width, [26], reciprocal to the PM in the analysis above); and
- given a desired and constant closed-loop torque bandwidth f_{BW} , faster valves are able to enlarge the Z-width.

VII. RESULTS & DISCUSSION

Thus far we presented: a) a new framework for representing the force dynamics transmitted to a load, which highlights the transmission stiffness; b) how to use this and other (e.g. rigid body) model information to design high-performance force and impedance controllers; and c) the influence of the valve dynamics on the torque controller performance and stability.

Some results regarding the performance of single controllers have already been presented within the previous sections. In this section, we aim to show more general results that demonstrate the performance of the overall impedance controlled HyQ leg as well as to present some practical issues that can strongly affect the performance of such controllers.

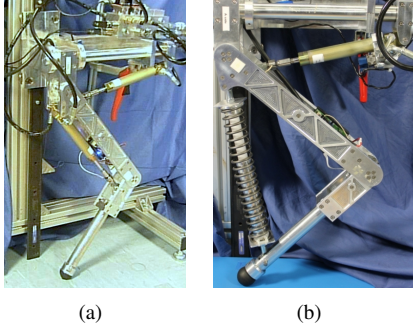


Fig. 13. HyQ leg fixed to a vertical slider. In (a) the traditional *actively-compliant* HyQ leg, and in (b) a specially-built version using a real spring-damper between the hip and the foot. The *passively-compliant* version of the leg was used exclusively for comparison and validation purposes.

A. Actively-compliant leg performance

To assess the HyQ impedance controller experimentally under high-frequency perturbations, a HyQ leg was fixed to a vertical slider (Fig. 13(a)) and dropped from a height of 25 cm onto a force plate, where the vertical ground reaction forces F_{GR} were measured. Then, the knee hydraulic cylinder, which has been programmed to emulate virtual elements, was replaced by a physical spring-damper (Fig. 13(b)) and the experiment was repeated. The leg weight was relevantly unaffected with this change. The virtual stiffness ($K_{vl} = 5250$ N/m), damping ($B_{vl} = 10$ Ns/m), and spring length ($l_{vl0} = 0.3$ m) were set to match the physical counterpart.

The impact forces and leg dynamics for both the active and passive case are compared in Fig. 14. It shows that the virtual spring-damper was able to qualitatively mimic the passive system. Taking the passively-actuated leg F_{GR} as reference, the actively-compliant leg presents an $RMSE = 137.77$ N (using the force plate measurements for both legs). Small differences in the stance period suggest that the leg with the virtual spring (red line and blue line) had on average a marginally smaller stiffness value than the real spring (black line), while the real spring (black line) has a higher impact force (around 1300 N) than the virtual spring (about 870 N). This result was not expected since factors such as actuator dynamics and sampling delay the virtual spring reaction and were expected to increase the impact forces. We believe factors such as small differences in the unsprung mass and nonlinearities in the real spring-damper assembly (e.g. backlash, static and Coulomb friction, and a non-ideal spring Hookean behaviour) might explain the slightly different dynamic behaviour and impact forces.

We also show the virtual spring stiffness during the first impact. The stiffness is calculated as $K_{vl} = f_{vl}/\Delta l_{vl}$, where the spring force f_{vl} is obtained by mapping the joint torques τ into the spring space by using the virtual spring Jacobian matrix (blue line in F_{GR} plot). The spring displacement variation Δl_{vl} is obtained with the joint encoders and leg direct kinematics. A maximum stiffness of 68 kN/m, which is about 13 times larger than the desired stiffness of 5.25 kN/m, can be observed a few milliseconds after the impact. However, the impedance controller quickly reacts and the virtual stiffness converges to the desired value in about 10 ms. We highlight that the main goal of our impedance controller is to set a desired dynamic

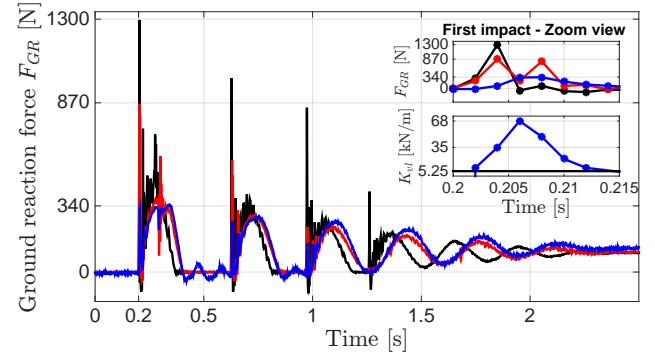


Fig. 14. Comparison of the actively-compliant leg dynamics (red and blue lines) with a passively-compliant version (black line) of the leg (Fig. 13(b)). We dropped both versions of the leg from 25 cm height on a force plate, which measured the vertical ground reaction forces F_{GR} . The red and black lines represent F_{GR} measured by the force plate, while the blue line shows F_{GR} calculated by mapping the joint torques into the end-effector space through the Jacobian transpose matrix. The ground reaction forces show that both systems bounce with very similar dynamics. A zoom view shows F_{GR} during the first impact and also the virtual leg stiffness K_{vl} , which reaches a peak of 68 kN/m and converges in about 10 ms to the desired value of 5.25 kN/m (black line). The data was sampled at 500 Hz.

behaviour to the robot (e.g. to emulate a spring-damper as in Fig. 13(b)) and not necessarily to obtain perfect stiffness tracking under high-frequency disturbances. Therefore, despite the inaccurate stiffness tracking under impacts, we consider such results very satisfactory given the similar overall behavior of the passively-compliant and actively-compliant legs.

B. Active vs. passive compliance

To complement the above experimental results, we now discuss some important aspects in the use of compliance in robotics and underline the *advantages and disadvantages* of both passive and active impedance. Such analysis is of fundamental importance for robot designers which have to decide in favor of one or the other, or even in a mix of both.

First of all, it should be clear that active impedance uses energy for producing the desired dynamic behaviour. Thus, this energy consumption may be a limiting factor for employing active impedance on robots that aim to be very energy efficient. On the other hand, energy efficiency is one of the hallmarks of passive compliance. Components such as springs can store energy while being compressed (or extended). In springs, the stored energy is proportional to the stiffness and to the *square* of the spring displacement. Hence, to maximize this stored energy, it is necessary to prioritize the spring compression over its stiffness. However, low stiffness reduces the joint controllability, leading usually to poor position tracking and maybe to dangerous situations in the worst case. For this reason and also due to design constraints, higher stiffness configurations are often preferred even though the energy storage capability is reduced. In these high stiffness configurations, the backdrivability and safety of the passive system are also drastically impaired. Finally, when the energy stored in the spring is suddenly released, it can result in high speed motions and a potentially risky situation for humans [39].

The application of passive impedance on a robot can be very cheap and simple. It can consist, for instance, of a simple layer

of rubber at the end-effector or of a linear spring in series with it [14]. However, more complex designs, such as VSAs [15], can substantially increase the costs and complexity of passive impedance. Active impedance is usually more expensive than traditional passive impedance. It commonly requires more hardware, such as force/torque sensors and data acquisition interfaces. Moreover, if the actively-compliant robot aims to perform highly-dynamic tasks, high-performance (and normally high-priced) hardware is also needed. HyQ, which uses high-bandwidth servovalves, is able to, for instance, perform a flying trot at roughly 2 m/s without any physical spring or damper in its mechanical structure. Although active impedance can be energy inefficient and possibly expensive due to its demands of high bandwidth sensing and actuation, it is much more *versatile*. An actively-compliant robot can take advantage of any programmable type of impedance (e.g. non-linear dampers, muscle-model-based springs, etc.) and vary the dynamic behaviour without needing physical changes. A more detailed discussion between the advantages and disadvantages of active and passive impedance can be found in [34], [31].

C. Load characteristics influence in torque control

It is not only the actuator bandwidth that determines the closed-loop torque control bandwidth. Other aspects also influence the performance of a joint torque controller, such as load friction and inertia. In general, the higher the value for these characteristics, the better the torque tracking.

Nonlinear friction forces, such as static and Coulomb, are very disadvantageous and undesirable in force control. Their discontinuities can cause stability problems. Viscous friction, on the other hand, can be very favourable to force control. It varies linearly with the velocity and introduces damping into the system, contributing to the stability.

The load inertia also plays an important role on the force control performance: the mass M_l works as a gain in the force open-loop dynamics (Eq. 4). Since this open-loop gain is also mapped to the closed-loop dynamics, higher inertias tend to provide higher control bandwidths. As generally robots have heavier links close to their base and the end-effector is as light as possible, proximal joints always tend to present a more satisfactory force tracking performance than distal joints. This is due to the negative gradient of the reflected inertia from the base to end-effector.

We verified the influence of the inertia on the force tracking capabilities of the HyQ leg through two experiments. Initially no additional load was added to the leg, but then a 2 kg weight was added to the foot. In both cases, a 2 Hz sinusoidal motion was performed with the leg in the air. The outer impedance loop used the joint-space PD position controller with inverse dynamics, and the inner force loop used the feedback linearization approach. The force loop was tuned individually for each joint to reach the maximum stable performance. The force tracking for the HFE and KFE joints is shown for both cases in Fig. 15(a) and Fig. 15(b). The dashed red line depicts the force reference, and the solid black line shows the actual force. These results confirm that larger reflected inertia in the joints results in better force tracking.

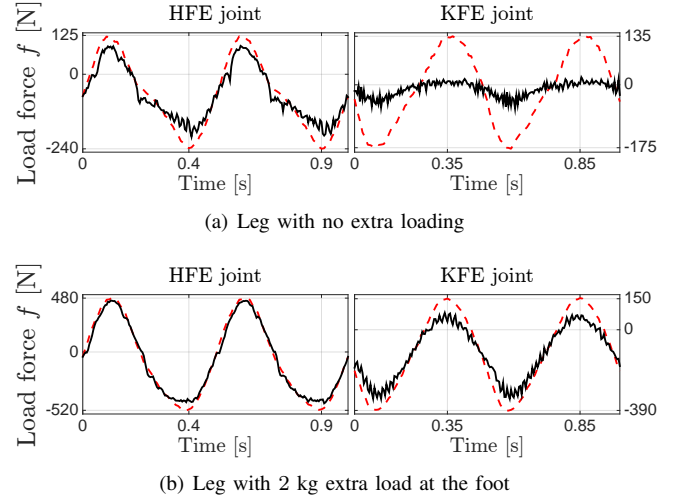


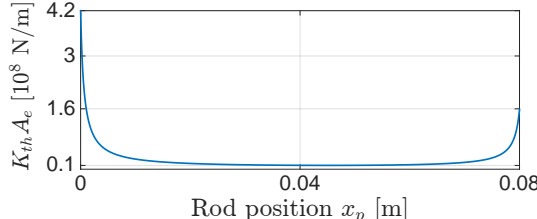
Fig. 15. HyQ joints force tracking for a 2 Hz sinusoidal motion and *different loads* on the foot. In each figure, the dashed red line represents the force reference created by the position controller and the solid black line the actual force. The HFE joint, which has a higher reflected inertia than the KFE joint, has always a better force tracking performance. Note the additional load improved the performance for both joints, particularly the KFE joint because of its substantial relative increase in inertia. The root-mean-square errors with respect to the amplitude of the reference force are $RMSE_{HFE} = 9.2\%$ and $RMSE_{KFE} = 27.3\%$ without load while $RMSE_{HFE} = 3.9\%$ and $RMSE_{KFE} = 11.2\%$ for the extra load case. The force controller gains were tuned individually to always provide the best stable performance.

D. Hydraulic transmission stiffness

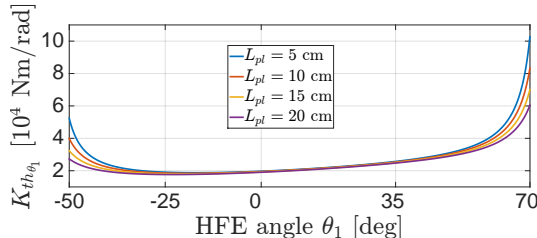
As we have seen in Section IV, the transmission stiffness is an important parameter in the force dynamics. Although the very low fluid compressibility makes the hydraulic transmission stiff, some design aspects such as the length and flexibility of the pipes can reduce this high stiffness [30]. Since HyQ uses rigid metal tubes between the valve and the actuator, we will not assess in this paper the effects of the pipe line flexibility on the hydraulic transmission stiffness.

Unlike real springs, which transform a displacement into force, hydraulic stiffness transforms a piston displacement into pressure. That is, the hydraulic stiffness unit is Pa/m. To obtain a stiffness in N/m, which has a more intuitive meaning, the stiffness K_{th} has to be multiplied by the equivalent actuator area A_e (Fig. 16(a)). This linear stiffness of the cylinder can also be mapped into joint space rotational stiffness $K_{th\theta}$ (Fig. 16(b)) by using the virtual work principle [40].

The stiffness magnitude at the minimum and maximum actuator positions depends directly on the pipe line volume that connects the valve to the cylinder chamber. The lower the pipe volume, the higher the stiffness (Fig. 16(b)). Thus, the pipe volume plays an important role in the controller and robot design and it must be taken into account when tuning the force gains and matching the transmission stiffness to the valve bandwidth. As we can see in Eq. 4, K_{th} is a gain into the system and the higher its value the higher the closed-loop force/torque bandwidth for a certain set of gains. Its relation with the *PM* and *Z-width* should be further investigated.



(a) Hydraulic transmission stiffness in cylinder space



(b) Rotational hydraulic stiffness in joint space

Fig. 16. (a) Hydraulic stiffness in cylinder space of HyQ cylinders for a rigid pipe of length $L_{pl} = 10$ cm and internal diameter $D_{pl} = 4$ mm. The hydraulic stiffness depends on the fluid properties, on the cylinder area, on the pipe length between the cylinder and valve, pipe flexibility, and on the cylinder rod position x_p . (b) Mapping of the hydraulic stiffness K_{th} into the rotational space of the HFE joint. The variable stiffness $K_{th\theta_1}$ defines how much torque is created when the HFE joint is moved with the valve blocked. This is equivalent to the stiffness of a rotational spring placed into the joint.

VIII. CONCLUSION

This paper has shown that through appropriate modelling and model-based control techniques high active impedance performance can be achieved in the limbs of a hydraulic robot such as HyQ. Many relevant aspects regarding the control and design of suitable force and compliance control architectures for robotics applications were presented.

We have shown through simulations and experiments that a feedback force PID controller presents a very limited response, and that a feed forward command can be used to compensate the effects of the load dynamics, considerably increasing the tracking capabilities. Also, through numerical analyses, we have shown that faster valves yields to more stable and faster closed-loop force controllers. Finally, through an experiment we demonstrated that heavier systems tend to present better force tracking performances.

As for the impedance control loop, we experimentally showed that our actively-compliant leg can qualitatively emulate a passive system. Although the desired impedance is not well tracked by the active system during the first milliseconds after the impact, the overall behaviour is very satisfactory. Also, the hydraulic actuators have demonstrated once more to be suitable for stiff actively-compliant systems since they safely withstand overloads and are fast enough to handle high-frequency disturbances.

Last but not least, having such torque-controlled machines will lead to a better understanding of how to build future robots, in particular helping to identify what impedance values and where in the robot passive elements should be used. This might make a robot more application-specific than versatile but, on the other hand, it would increase energy efficiency.

Future work will aim to establish a method for choosing the most suitable stiffness for the robot according to the task requirements; to design a robust and adaptive controller for low-level hydraulic force control since some parameters are difficult to estimate or even change during the task, e.g. viscosity of the oil that is highly dependent on its temperature; to develop an accurate model for the friction in the hydraulic cylinders, which could be used in the model-based controller; to experimentally evaluate valves that are more energy efficient, but with lower bandwidth.

ACKNOWLEDGEMENTS

Most of this research has been performed when T.B. and J.B. were at the Fondazione Istituto Italiano di Tecnologia (IIT). This research has been supported by IIT, Swiss National Science Foundation professorship to J.B., and BALANCE Project (Grant 601003 of the EU FP7 program).

REFERENCES

- [1] N. Hogan, "Impedance control: An approach to manipulation: Part II – Implementation," *ASME, Transactions, Journal of Dynamic Systems, Measurement, and Control*, vol. 107, pp. 8–16, 1985.
- [2] J. Pratt, C. Chew, A. Torres, P. Dilworth, and G. Pratt, "Virtual model control: An intuitive approach for bipedal locomotion," *The International Journal of Robotics Research*, vol. 20, no. 2, pp. 129–143, 2001.
- [3] O. Khatib, "A unified approach for motion and force control of robot manipulators: The operational space formulation," *IEEE Journal of Robotics and Automation*, vol. 3, no. 1, pp. 43–53, 1987.
- [4] M. Mistry, J. Buchli, and S. Schaal, "Inverse dynamics control of floating base systems using orthogonal decomposition," *IEEE Int. Conference on Robotics and Automation (ICRA)*, pp. 3406–3412, 2010.
- [5] J. Buchli, M. Kalakrishnan, M. Mistry, P. Pastor, and S. Schaal, "Compliant quadruped locomotion over rough terrain," in *Proceedings of IEEE/RSJ International Conference on Intelligent Robots and Systems (IROS)*, 2009, pp. 814–820.
- [6] A. D. Luca, A. Albu-Schaffer, S. Haddadin, and G. Hirzinger, "Collision detection and safe reaction with the dlr-iii lightweight manipulator arm," in *IEEE/RSJ International Conference on Intelligent Robots and Systems*, oct. 2006, pp. 1623 –1630.
- [7] T. Boaventura, M. Focchi, M. Frigerio, J. Buchli, C. Semini, G. Medrano-Cerda, and D. Caldwell, "On the role of load motion compensation in high-performance force control," in *IEEE/RSJ International Conference on Intelligent Robots and Systems (IROS)*, oct. 2012, pp. 4066 –4071.
- [8] C. Semini, N. G. Tsagarakis, E. Guglielmino, M. Focchi, F. Cannella, and D. G. Caldwell, "Design of HyQ - a hydraulically and electrically actuated quadruped robot," *IMechE Part I: J. of Systems and Control Engineering*, vol. 225, no. 6, pp. 831–849, 2011.
- [9] T. Boaventura, C. Semini, J. Buchli, M. Frigerio, M. Focchi, and D. G. Caldwell, "Dynamic torque control of a hydraulic quadruped robot," in *IEEE International Conference in Robotics and Automation (ICRA)*, 2012, pp. 1889–1894.
- [10] T. Boaventura, G. Medrano-Cerda, C. Semini, J. Buchli, and D. Caldwell, "Stability and performance of the compliance controller of the quadruped robot hyq," in *IEEE/RSJ International Conference on Intelligent Robots and Systems (IROS)*, 2013.
- [11] T. Boaventura, "Hydraulic compliance control of the quadruped robot hyq." Ph.D. dissertation, Istituto Italiano di Tecnologia and Univerty of Genoa, Italy, 2013.
- [12] M. T. Mason, "Compliance and force control for computer controlled manipulators," *IEEE Transactions on Systems, Man and Cybernetics*, vol. 11, no. 6, pp. 418 –432, june 1981.
- [13] D. E. Whitney, "Historical perspective and state of the art in robot force control," in *IEEE International Conference on Robotics and Automation (ICRA)*, vol. 2, mar 1985, pp. 262 – 268.
- [14] G. Pratt and M. Williamson, "Series elastic actuators," in *IEEE International Conference on Intelligent Robots and Systems (IROS)*, 1995.
- [15] B. Vanderborght, A. Albu-Schaeffer, A. Bicchi, E. Burdet, D. G. Caldwell, R. Carloni, M. G. Catalano, O. Eiberger, W. Friedl, G. Ganesh, M. Garabini, M. Grebenstein, G. Grioli, S. Haddadin, H. Hopfner, A. Jafari, M. Laffranchi, D. Lefèber, F. Petit, S. Stramigioli, N. G. Tsagarakis, M. V. Damme, R. V. Ham, L. C. Visser, and S. Wolf, "Variable impedance actuators: A review," *Robotics and Autonomous Systems*, vol. 61, no. 12, pp. 1601–1614, 2013.

- [16] S. H. Hyon, "A motor control strategy with virtual musculoskeletal systems for compliant anthropomorphic robots," *IEEE/ASME Transactions on Mechatronics*, vol. 14, pp. 677–688, 2009.
- [17] A. Albu-Schäffer, C. Ott, and G. Hirzinger, "A unified passivity-based control framework for position, torque and impedance control of flexible joint robots," *The International Journal of Robotics Research*, vol. 26, no. 1, pp. 23–29, 2007.
- [18] G. Bilodeau and E. Papadopoulos, "A model-based impedance control scheme for high-performance hydraulic joints," in *Intelligent Robots and Systems, 1998. Proceedings., 1998 IEEE/RSJ International Conference on*, vol. 2, Oct 1998, pp. 1308–1313 vol.2.
- [19] I. Davliakos and E. Papadopoulos, "Impedance model-based control for an electrohydraulic stewart platform," *European Journal of Control*, pp. 560–577, 2009.
- [20] L. Villani and J. De Schutter, "Force control," in *Springer Handbook of Robotics*. B. Siciliano and O. Khatib, Eds. Springer Berlin Heidelberg, 2008, pp. 161–185.
- [21] S. Eppinger and W. Seering, "Three dynamic problems in robot force control," in *Robotics and Automation, 1989. Proceedings., 1989 IEEE International Conference on*, May 1989, pp. 392–397 vol.1.
- [22] W. T. Townsend, "The effect of transmission design on force-controlled manipulator performance," *Technical Report 1054*, 1988.
- [23] F. Conrad and C. Jensen, "Design of hydraulic force control systems with state estimate feedback," in *IFAC 10th Triennial Congress*, Munich, Germany, 1987, pp. 307–31.
- [24] S. Dyke, B. Spencer Jr., P. Quast, and M. Sain, "Role of control-structure interaction in protective system design," *Journal of Engineering Mechanics, ASCE*, vol. 121 No.2, pp. 322–38, 1995.
- [25] A. Alleyne, R. Liu, and H. Wright, "On the limitations of force tracking control for hydraulic active suspensions," in *Proceedings of the American Control Conference*, vol. 1, jun 1998, pp. 43 –47 vol.1.
- [26] J. E. Colgate and J. M. Brown, "Factors affecting the z-width of a haptic display," in *IEEE International Conference on Robotics and Automation (ICRA)*, 1994, pp. 3205–3210.
- [27] J. E. Colgate and G. G. Schenkel, "Passivity of a class of sampled-data systems: Application to haptic interfaces," *Journal of Robotic Systems*, vol. 14, no. 1, pp. 37–47, 1997.
- [28] S. Hirose, K. Ikuta, and Y. Umetani, "Development of a shape memory alloy actuators. performance assessment and introduction of a new composing approach," *Advanced Robotics*, vol. 3, no. 1, pp. 3–16, 1989.
- [29] S. Peng, D. T. Branson, E. Guglielmino, T. Boaventura, and D. G. Caldwell, "Performance assessment of digital hydraulics in a quadruped robot leg," in *Proceedings of the 11th Biennial Conference on Engineering Systems design and Analysis ESDA11*, 2012.
- [30] H. E. Merritt, *Hydraulic control systems*. Wiley-Interscience, 1967.
- [31] C. Semini, V. Barasuol, T. Boaventura, M. Frigerio, M. Focchi, D. G. Caldwell, and J. Buchli, "Towards versatile legged robots through active impedance control," *The International Journal of Robotics Research (IJRR)*, vol. 34, no. 7, pp. 1003–1020, 2015.
- [32] V. Barasuol, J. Buchli, C. Semini, M. Frigerio, E. De Pieri, and D. Caldwell, "A reactive controller framework for quadrupedal locomotion on challenging terrain," in *Robotics and Automation (ICRA), 2013 IEEE International Conference on*, May 2013, pp. 2554–2561.
- [33] MOOG Inc., *Data Sheet of E024 Series Microvalve*, 2003.
- [34] W. Wang, R. N. Loh, and E. Y. Gu, "Passive compliance versus active compliance in robot-based automated assembly systems," *Industrial Robot: An International Journal*, vol. 25, Iss: 1, pp. 48–57, 1998.
- [35] R. Featherstone and D. Orin, "Robot dynamics: equations and algorithms," in *IEEE International Conference on Robotics and Automation (ICRA)*, vol. 1, 2000, pp. 826 –834 vol.1.
- [36] J. Buchli, F. Stulp, E. Theodorou, and S. S., "Learning variable impedance control," *Int. Journal of Robotics Research*, 2011, in print.
- [37] A. Hajimiri, "Generalized time- and transfer-constant circuit analysis," *IEEE Trans. on Circuits and Systems*, vol. 57-I, no. 6, pp. 1105–1121, 2010.
- [38] W. Chen, *The VLSI Handbook*, ser. Electrical Engineering Handbook. CRC Press, 2010.
- [39] B. Vanderborght, *Dynamic Stabilisation of the Biped Lucy Powered by Actuators with Controllable Stiffness*, ser. Springer Tracts in Advanced Robotics. Springer, 2010.
- [40] L. Sciavicco and B. Siciliano, *Modelling And Control Of Robot Manipulators*. Springer, 2001.



Thiago Boaventura received his B.Sc. and M.Sc. degrees in Mechatronic Engineering from the Federal University of Santa Catarina, Brazil, in 2009. He received his Ph.D. degree in Robotics, Cognition, and Interaction Technologies from a partnership between the Italian Institute of Technology and University of Genoa, Italy, in 2013.

He is currently a post-doctoral researcher at the Agile & Dexterous Robotics Lab, at ETH Zurich, in Switzerland. He is mainly involved in the EU FP7 BALANCE project with focus in the collaborative impedance control of exoskeletons. His research interests include impedance and admittance control, model-based control, legged robotics, optimal and learning control, and wearable robotics.



Jonas Buchli holds a Diploma in Electrical Engineering from ETH Zurich (2003) and a PhD from EPF Lausanne (2007). From 2007 to 2010 he was a Post-Doc at the Computational Learning and Motor Control Lab at the University of Southern California, where he was the team leader of the USC Team for the DARPA Learning Locomotion challenge. From 2010-12 he was a Team Leader at the Advanced Robotics Department of the Italian Institute of Technology in Genoa. Jonas Buchli has received a Prospective and an Advanced Researcher Fellowship from the Swiss National Science Foundation (SNF). In 2012 he received a Professorship Award from the SNF. He is currently an Assistant Professor at the Institute of Robotics and Intelligent Systems at ETH Zurich and director of the Agile & Dexterous Robotics Lab.



Claudio Semini Claudio Semini is the head of the Dynamic Legged Systems lab of the Department of Advanced Robotics at Istituto Italiano di Tecnologia (IIT). He holds an MSc degree from ETH Zurich in electrical engineering and information technology (2005). From 2004 to 2006 he first visited the Hirose Lab at the Tokyo Institute of Technology, followed by work on mobile service robotics at the Toshiba R&D center in Kawasaki, Japan. During his doctorate from 2007-2010 at the IIT he designed and constructed the quadruped robot HyQ and worked

on its control. After a post-doc in the same department, in 2012, he became the head of the Dynamic Legged Systems lab. His research focus lies on the construction and control of highly dynamic and versatile legged robots in real-world environments.



Darwin G. Caldwell received the B.S. and Ph.D. degrees in robotics from the University of Hull, Hull, U.K., in 1986 and 1990, respectively, and the M.Sc. degree in management from the University of Salford, Salford, U.K., in 1996. He is currently the Director of Robotics at the Italian Institute of Technology, Genoa, Italy.

He is a Visiting/Honorary/Emeritus Professor at the University of Sheffield, the University of Manchester, and the University of Wales, Bangor. His research interests include innovative actuators and sensors, haptic feedback, force augmentation exoskeletons, dexterous manipulators, humanoid robotics, biomimetic systems, rehabilitation robotics, and telepresence procedures.